Accepted Manuscript

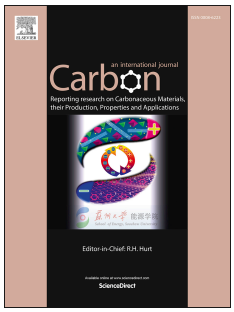

From waste to wealth: From Kraft lignin to free-standing supercapacitors

Philipp Schlee, Omid Hosseinaei, Darren Baker, Alice Landmer, Per Tomani, M.J. Mostazo-Lopez, Diego Cazorla-Amorós, Servann Herou, Maria-Magdalena Titirici

PII: S0008-6223(19)30036-3

DOI: https://doi.org/10.1016/j.carbon.2019.01.035

Reference: CARBON 13839

To appear in: *Carbon*

Received Date: 25 October 2018

Revised Date: 17 December 2018

Accepted Date: 8 January 2019

Please cite this article as: P. Schlee, O. Hosseinaei, D. Baker, A. Landmer, P. Tomani, M.J. Mostazo-Lopez, D. Cazorla-Amorós, S. Herou, M.-M. Titirici, From waste to wealth: From Kraft lignin to free-standing supercapacitors, *Carbon* (2019), doi: https://doi.org/10.1016/j.carbon.2019.01.035.

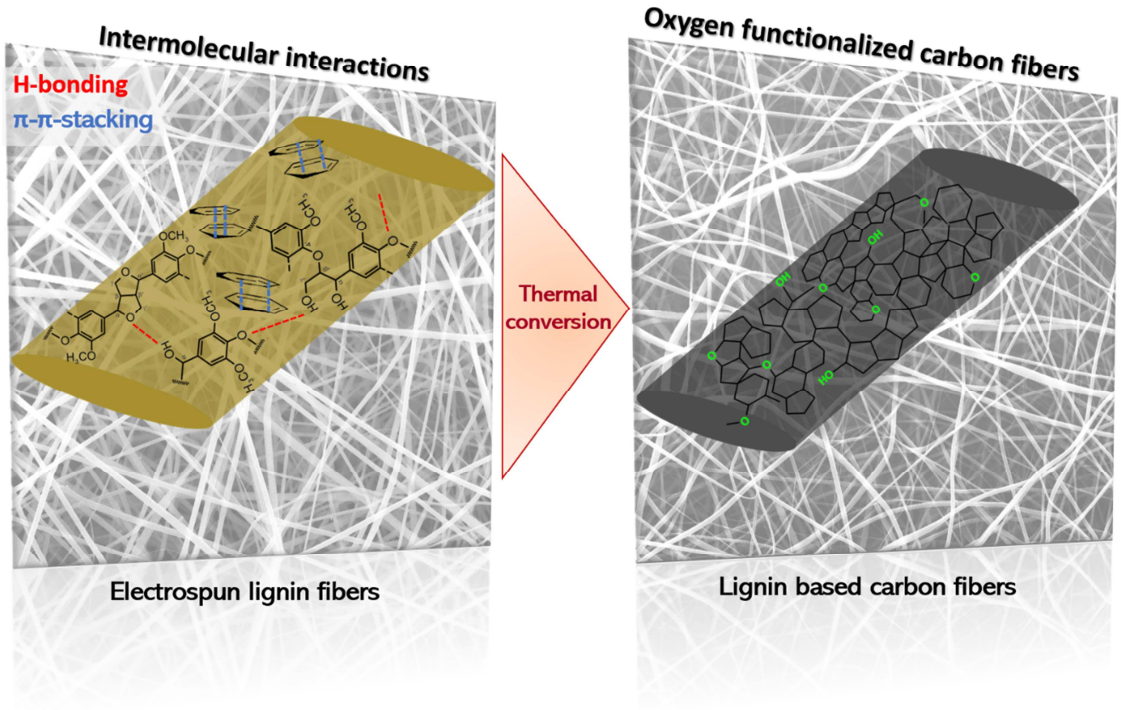

From Waste to Wealth: From Kraft Lignin to Free-standing Supercapacitors

Philipp Schlee[1,2], Omid Hosseinaei[3], Darren Baker[3], Alice Landmer[3], Per Tomani[3], M. J. Mostazo-Lopez[4], Diego Cazorla-Amorós[4], Servann Herou[1,2], Maria-Magdalena Titirici[1,2*]

[1] Queen Mary University of London, School of Engineering and Materials Science, Mile End Road, E1 4NS, London, UK

[2] Materials Research Institute, Queen Mary University of London, Mile End Road, E1 4NS, London, UK

[3] RISE Bioeconomy, Drottning Kristinas väg 61 Stockholm, Sweden

[4] Departamento de Química Inorgánica, Universidad de Alicante, Apartado 99, E-03080 Alicante, Spain

* Corresponding Author. Tel.: 020 7882 6272. E-mail: m.m.titirici@qmul.ac.uk (Maria-Magdalena Titirici)

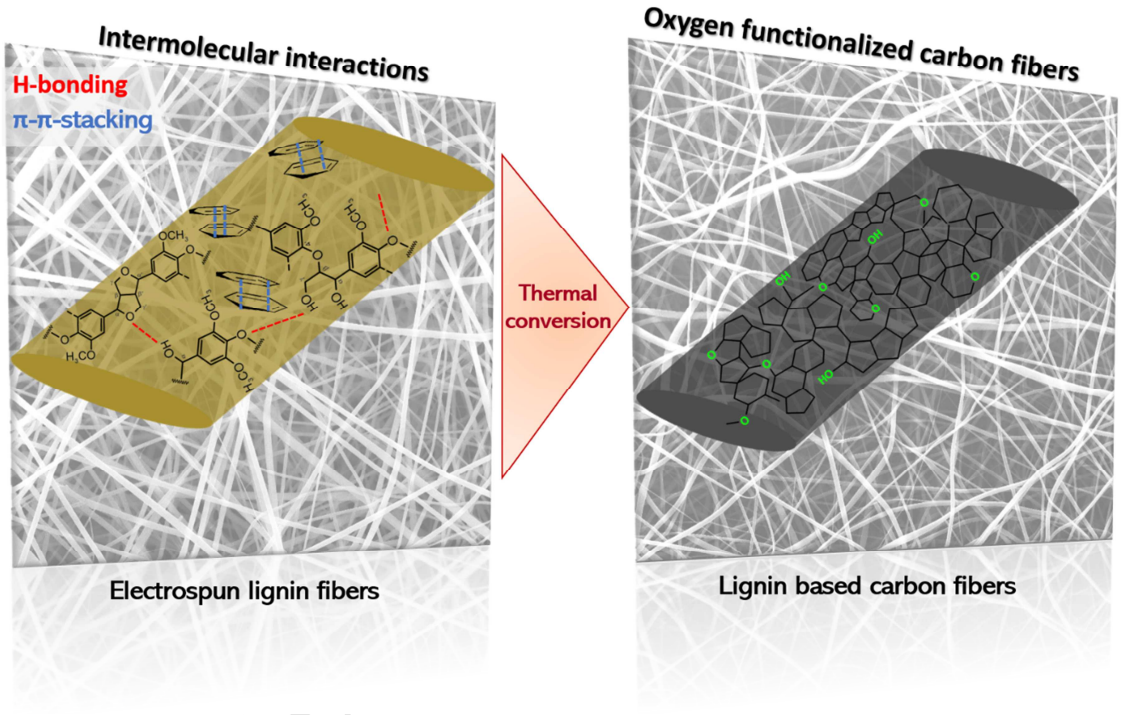

Abstract

Pure eucalyptus Kraft lignin derived carbon fiber mats were produced based on a model workflow. It covers the preparation and characterization of the lignin precursor and the carbon materials and its testing in the final application (supercapacitor). Sequential solvent extraction was employed to produce a eucalyptus Kraft lignin precursor which could be electrospun into

lignin fibers without any additives. The fiber formation from low molecular weight lignin is assigned to strong intermolecular interactions via hydrogen bonding and π-π-stacking between individual lignin macromolecules which gives rise to association complexes in the electrospinning solution. By stabilization in air, carbonization in N_2 and an activation step in CO_2, free-standing microporous carbon fiber mats could be produced. These fiber mats possess mainly basic oxygen functional groups which proved to be beneficial when tested as free-standing electrodes in symmetric supercapacitors. Consequently, the CO_2-activated fiber mats showed a high specific gravimetric capacitance of 155 F/g at 0.1 A/g, excellent rate capability with 113 F/g at 250 A/g and good capacitance retention of 94% after 6000 cycles when tested in 6 M KOH electrolyte. Therefore, we conclude that lignin itself is a promising precursor to produce microporous, oxygen functionalized carbon fibers serving as free-standing electrodes in aqueous supercapacitors.

1. Introduction

Lignin is the generic term for a large group of aromatic polymers resulting from the oxidative combinatorial coupling of 4-hydroxyphenylpropanoid units (Figure 1).[1,2] It is the second most abundant biopolymer on Earth and can be found in the plants' cell walls giving plants their structural integrity.[2,3] Moreover, lignin is essential for the water transport and acts as barrier against pathogens and herbivores.[4,5] Finally, its random and branched structure results in reluctance to (bio-)chemical or physical degradation.[5] This structural and chemical randomness, optimized by Nature over 100 millions years, is the main obstacle for its use as a precursor for advanced functional (carbon) materials.[6–8]

Kraft lignin differs structurally and chemically considerably from native lignin due to the extraction process while its complexity is preserved and even enhanced.[8]

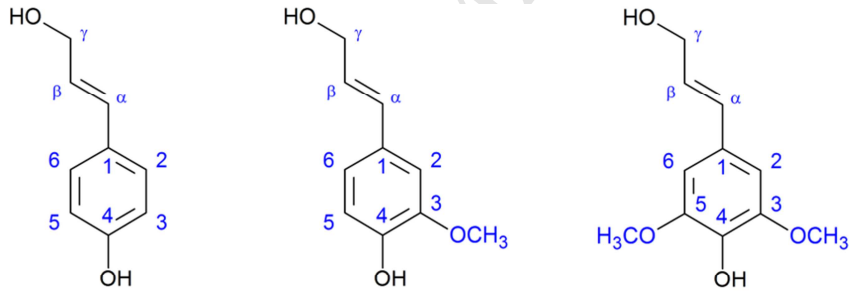

Figure 1 Basic building units of lignins which differ in their degree of methoxylation.

It is isolated in large quantities (70 million tons p.a.) via the Kraft process which separates cellulose and hemicellulose from lignin by treatment in a digester with a strong base and sodium sulfite at elevated temperatures and pressures.[8,9] To date, the majority of the Kraft lignin isolated globally is incinerated to produce steam and heat for energy use.[10] However, from an economic standpoint the potential of Kraft lignin is by far not fully exploited and hence, lignin is considered an undervalued by-product of the pulp and paper making.[11] This makes it an

economically and ecologically attractive feedstock for the manufacture of functional carbon materials. Carbons are widely used in various technologies and applications due to their physical and chemical versatility.[12–14] For instance, the most widespread electrochemical energy storage system, namely Li ion batteries (LIBs), and the upcoming Na ion batteries (NIBs) rely on carbon anodes.[15–17] Fuel cells and metal air batteries also heavily rely on carbon materials as active material or support of electrocatalysts.[18–21] Finally, electric double layer supercapacitors (SCs) constitute another more rapid form of energy storage in which carbon materials play a crucial role by providing surface sorption sites for charge storage.[22–24] Many of these energy storage devices are based on unsustainable, petroleum derived carbon materials prepared under harsh conditions (CVD, Hummer's method, etc.).[25] In the case of supercapacitors, these are typically coated on metal foil/grid with an insulating binder and conductive additive to form the electrodes.[25,26] This gives rise to resistive interfaces between the active material (activated carbon powder) and the current collector.[26,27] Besides, additional interfaces are created within the film due to the separation of the conductive material by the insulating binder.[26] Non-flexible and bulky devices are the consequence of the state-of-the-art electrodes.[28] Replacing these by free-standing and flexible electrodes gives the opportunity to omit current collectors, insulating binders and conductive additives, as free-standing electrodes constitute both the active material and the current collector.[28] Furthermore, building in flexibility would allow energy storage devices to be molded around electrical vehicles or portable electronics, thus significantly reducing their weight and bulk volume. Indeed, recently, lignin derived carbon nanofiber (CNF) mats were shown to be well-suited as free-standing and even flexible electrodes in SCs.[29–33]

However, literature on the relation between the structure/chemistry of the lignin precursor and the resulting materials' properties is very scarce to date. Since lignin is not a well-established ("off-the-shelf ") chemical, but inherently a loosely defined precursor, it is crucial to characterize the lignin used as precursor to understand its structural and chemical features. As mentioned previously, lignin is a generic name for a big family of biopolymers containing aromatic units linked differently. Hence, every lignin is different. Neglecting this, will give rise to a *potpourri* of non-comparable works and irreproducible materials portfolios which will substantially hinder progress towards lignin-based commercial products. Here, we address this literature gap by providing a model workflow (Figure 2) whereby the properties of the initial lignin precursor are linked with the properties of the resulting carbon fibers.

We report purely Kraft lignin derived fiber mats prepared via electrospinning without using any additional synthetic polymer. Throughout stabilization in air and carbonization in nitrogen the Kraft lignin fiber mat was converted to a carbon fiber (CF) mat. Additionally, the pore size distribution (PSD) was optimized by CO_2 activation to optimize performance as free-standing SC electrodes. Based on the lignin structure/chemistry and final CF properties the potential of lignin as a suitable natural precursor for porous carbon fiber mats can be investigated without interfering effects from additives or co-polymers.

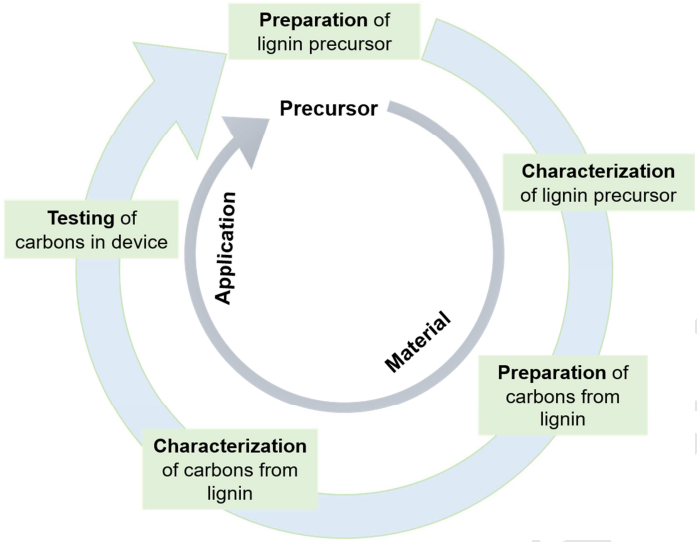

Figure 2 Workflow for the use of lignin as a precursor for carbon materials.

2. Materials and Methods

2.1. Preparation of lignin precursor

The eucalyptus Kraft lignin was isolated using the LignoBoost process at RISE Innventia AB (Stockholm, Sweden). The black liquor, from eucalyptus wood, was obtained from the ENCE pulp mill (Huelva, Spain). The isolated lignin was dried at 80 °C under vacuum for about 24 h. A sequential solvent extraction was used to produce a suitable lignin fraction for electrospinning. The solvent extraction method was a modified version of the method described elsewhere.[34,35] At first, the dry lignin (1000 g) was extracted with deionized water by rapidly stirring in 10 L water at 60 °C for 2 h. The suspension was cooled to room temperature and then filtered. The recovered air-dried solid was dried at 80 °C under vacuum for about 12 h. Subsequently, the lignin was extracted with dichloromethane, by stirring in 10 L solvent at room temperature for 2 h. Afterwards, the sample was filtrated and the solid recovered on the filter and extracted using methanol (1:10 solid to liquid ratio, room temperature, 4 h). The extract solution was then filtered, and lignin from the filtrate was isolated using a rotary evaporator. The isolated lignin

was dried in a vacuum oven at 80 °C for 12 h. The final yield for this fraction used as precursor for electrospinning was 52.3%.

2.2. Characterization of lignin precursor

2.2.1. Ash content and composition of the extracted lignin

The ash content and composition of the extracted lignin sample were determined using standard methods.[36–39] In brief, the ash content was determined by combustion of the lignin sample at 575 °C. The compositional analysis was performed by two step acid hydrolysis and measurement of lignin and carbohydrate content. Lignin content was measured as acid soluble and acid insoluble lignins by gravimetric method and UV spectroscopy. Carbohydrates were measured using high-performance liquid chromatography (HPLC). Due to the high purity of the lignin sample, impurities (carbohydrates and ash) were used to determine the purity of the sample.

2.2.2. Elemental (CHNS/O) analysis

The organic content of the lignin was measured using a PerkinElmer 2400II CHNS/O combustion elemental analyzer based on the Pregl-Dumas method.[40] The absolute content of C, H, N and S were measured. The oxygen content was calculated as 100% minus the sum of C, H, N, S, and ash.

2.2.3. Determination of glass transition temperature

The glass transition temperature (T_g) was determined in triplicate on approximately 3 mg samples of lignin using a TA Instruments Q2000 differential scanning calorimeter (DSC). Each specimen was heated from 25 °C at a rate of 20 °C/min under nitrogen (50 ml/min) to 150 °C and held at that temperature for 5 minutes, to remove any remaining moisture, then cooled to 25 °C and again heated to 220 °C at the same heating rate. The second trace was used for the calculation of the T_g.

2.2.4. Determination of molecular weight

The molecular weight distribution was determined by size exclusion chromatography (SEC) using a Water SEC system equipped with UV (set at 280 nm) and RI detectors. Two PSS MCX columns (1000 and 100000 Å) were connected in series. The mobile phase was a pH 12 buffer solution at a flow rate of 0.5 ml/min. Lignin sample was dissolved in NaOH solution (pH = 13.5) and diluted to a suitable concentration with the mobile phase. The injection volume was 100 µL. The SEC system was calibrated using polystyrene standards with the molecular weight in the range of 891 to 780000 g/mol.

2.2.5. NMR spectroscopy

NMR experiments were performed using a Bruker Avance III 400MHz NMR spectrometer equipped with a broadband PFG 5 mm probe at room temperature (25 °C). For 2D (HSQC) spectroscopy, 100 mg of lignin were dissolved in 0.75 ml of DMSO-d_6. NMR spectra were recorded using the Bruker's "hsqcetgpsisp2.2" pulse program (adiabatic-pulse) with 1.5 s pulse delay. The number of transients was 64 and 256 time increments and were recorded in the ^{13}C dimension. The $^{1}J_{CH}$ used was 145 Hz. Data processing and analysis was performed using Bruker's Topspin 4.0. The central solvent peak was used as an internal reference (δ_C/δ_H 39.5/2.49 ppm). HSQC cross-signals were assigned by correlation with literature databases. [7,41–44] Hydroxyl groups were measured using quantitative ^{31}P NMR spectroscopy after derivatization of lignin with 100 µL of 2-chloro-4,4,5,5-tetramethyl-1,3,2-dioxaphospholane (TMDP). [45,46] The lignin sample (30 mg) was dissolved in dimethylformamide/pyridine (1:1 v/v) and mixed with 100 µL of a solution of *N*-hydroxy-5-norbornene-2,3-dicarboxylic acid imide (20 mg/ml) and chromium(III) acetylacetonate (5 mg/ml) as internal standard and relaxation agent, respectively. ^{31}P NMR spectra were acquired using an inverse-gated decoupling pulse sequence with a 90 ° pulse angle, 10 s relaxation delay, and 512 scans.

2.3. Preparation of carbon fiber mats from lignin

The precursor solutions for electrospinning contained 50 wt% fractionated eucalyptus hardwood Kraft lignin (Rise AB, Stockholm) dissolved in DMF (VWR). These solutions were typically sonicated for 90 min and repeatedly shaken for several minutes and finally stirred for several days in a sealed glass vial until a homogeneous solution was obtained. For one electrospinning run, a plastic syringe (Plastipak luer-lock, 5 ml) was loaded with 2 ml of the solution. The syringe was discharged at a rate of 1 ml/hr with a single syringe infusion pump (KDS-100-CE, KD Scientific). A high voltage between the syringe needle (gauge = 22, Hamilton) and a rotating collector was applied with a transformer (Glassmann high voltage inc., USA). The collector was placed 13 cm away from the needle's tip and the rotating speed was 72 rpm. Electrospinning was carried out in a room with an air conditioning system to control humidity at 30% (±5%). After spinning, the as-spun lignin fiber mats were converted to carbon fiber mats by a two-step thermal treatment: 1) stabilization in synthetic air (300 ml/min) and 2) carbonization in N_2 (300 ml/min) in a quartz tube furnace (OTF-1200X, MTI). Hereby, the lignin fiber mats were stabilized at 250 °C for 15 min, where the ramp between RT and 50 °C was 10 °C/min and the one between 50 and 250 °C was 0.5 °C/min. Subsequently, the fiber mats were carbonized at 900°C for 30 min, where the ramp between RT and 250 °C was 2.5 °C/min and the one between 250 and 900 °C was 3 °C/min. Additionally, some of the carbon fiber mats were further activated at 800 °C in CO_2 (200 ml/min) for 60 min. The heating rate was 5 °C/min.

2.4. Characterizations of carbon fiber mats

2.4.1. Morphological characterization

Fiber morphology was characterized using a FEI Inspect F scanning electron microscope (SEM) with an accelerating voltage of 20 kV. Both as-spun and carbonized fiber samples were gold

coated prior to imaging. Fiber diameter distributions were generated from SEM images using the ImageJ software package (U.S. National Institutes of Health). Diameters are reported as the mean and standard deviation based on measurements of 100 fibers.

TEM images were recorded with a JEOL 2010 operated at 200 kV.

2.4.2. Surface chemical composition: Temperature programmed desorption (TPD)

Temperature programmed desorption (TPD) experiments were carried out in a TGA-DSC instrument (TA Instruments, SDT Q600 Simultaneous) coupled to a mass spectrometer (Thermostar, Balzers, GSD 300 T3) by heating the samples (approx. 4 mg) up to 950 °C (heating rate: 20 K/min) under helium atmosphere (flow rate: 100 ml/min). The thermobalance was purged for 2 hours under helium atmosphere prior to the heating of the sample. The calibration of the equipment for H_2O, CO and CO_2 evolved gases was carried out using the decomposition of a calcium oxalate (99.999%, Sigma Aldrich) standard.

2.4.3. Porosity measurements

The surface areas and pore size distributions of the carbonized fiber mats were determined by N_2 and CO_2 ad-/desorption measurements at 77 K and 273 K, respectively, using an Autosorb iQ (Quantachrome Instruments, US). Samples were degassed at 473 K for 16 h under vacuum (0.27 Pa) before analysis. Pore size distributions were calculated by Non-Localized Density Functional Theory (NLDFT) for CO_2 sorption and Quenched Solid State DFT (QSDFT) for N_2 sorption.

2.5. Testing of carbon fiber mats in supercapacitors

The Kraft lignin derived CF mats were tested as electrodes in symmetric supercapacitor cells. All measurements were performed in a two-electrode set-up consisting of two similar carbon electrodes (symmetric SC type). The SCs were assembled in a Swagelok-type cell and connected

to a VSP-potentiostat (Biologic, France). The electrolyte was 6 M KOH and as a separator standard filter paper was used (Whatman, GE Healthcare Life Sciences, UK, Grade GF/D). Before the actual measurements, the cells were galvanostatically charged and discharged for 500 cycles to ensure wetting of the electrodes with the electrolyte. Subsequently, cyclic voltammetry (CV) and galvanostatic charge-discharge with potential limitation (GCD) were carried out at different rates. Impedance spectroscopy was conducted at open circuit potential and with an amplitude of 5 mV in a frequency range of 10 mHz to 500 kHz. Finally, capacitance retention was measured at a rate of 5 A/g for 6000 cycles.

3. Results and Discussion

3.1. Lignin characterization

After the preparation of the lignin precursor (described in 2.1), the resulting extracted lignin was characterized according to the model workflow in Figure 2. The elemental composition of the lignin summarized in Table 1 shows low amounts of ash and residual carbohydrates. The purity is higher than what has been reported for non-fractionated Kraft and organosolv lignins.[43,47,48] The solvent extraction of lignin eliminates impurities and results in increased purity of lignin as most impurities are not soluble in the solvents used and hence remain in the insoluble fraction.[34,49] Elemental analysis shows the presence of sulphur in the lignin, as a result of Na_2S in the Kraft process, which is common in Kraft lignins.[43,48] It is difficult to remove sulphur entirely from these lignins since it is covalently bound within the lignin structure. The lignin has a high carbon content of 62.2 wt% which potentially could give high carbonization yield. The presence of heteroatoms, especially oxygen, indicates formation of pores after carbonization of the lignin-based fibers.

Table 1 Composition of extracted eucalyptus Kraft lignin.

Component	Composition (%)
Carbohydrates	0.40
Ash	0.27
Purity	99.3
C	62.2
H	5.56
N	0.17
O	29.7
S	2.06

[1] Purity was determined by subtracting carbohydrates and ash content from the dry weight of lignin.

Additionally, the inorganic elemental content determined by Inductively Coupled Plasma – Optical Emission Spectroscopy (ICP-OES) shows that sodium and sulfur are the major impurities (Figure S1). These elements originate from the Kraft pulping process. The other elements have a low concentration. Inorganic elements in general catalyze the gasification of carbon and are an explanation of low yields and generation of pores.[50,51] Since the amount and type of inorganic impurities are not controllable they should be reduced to a minimum which was achieved here. The fractionated lignin has a T_g of 154 °C (Table S1, Figure S2) which is higher than reported values for non-fractionated hardwood Kraft lignin and pH-fractionated eucalyptus Kraft lignin.[52–55] The relatively high T_g of this lignin indicates higher molecular weight of this fraction as a result of removing some of the lower molecular weight components during first extraction.[56] Lignin with higher T_g potentially can stabilize at faster rate and reduce the production time of carbon fibers.[34,57] This is particularly important in the case of hardwood lignins which generally require slower stabilization rate compared to softwood lignins.[55,57] The thermal decomposition profile is shown in Figure S3. A summary of key data related to it is shown in Table S1. Lignin has a thermal decomposition temperature of 250 °C with a maximum

thermal degradation rate at 359 °C. In addition, the lignin precursor has higher residual char (38.3%) compared to pH-fractionated eucalyptus Kraft lignin.[53] The char yield correlates with carbon yield during carbonization which is 33.1% shown in Table 2.

The molecular weight values are 1900 g/mol (M_w) and 1200 g/mol (M_n). It is difficult to compare absolute molecular weight values for lignins due to the variability in measurement methods. However, the (poly-)dispersity index (PD) is relatively low (1.5) compared to what has been reported on fractionated and non-fractionated hardwood Kraft lignin. [52,53] This indicates that a homogenous and narrow molecular weight fraction of lignin was obtained by the sequential solvent extraction.

The ^{31}P NMR spectrum and the corresponding hydroxyl group distribution of the lignin sample are presented in Figure S4 and Figure 3, respectively. The number of hydroxyl groups are close to the data previously reported for eucalyptus and other hardwood lignins.[47,58] However, this fraction has a relatively lower number of aliphatic hydroxyl groups, compared to non-fractionated eucalyptus Kraft and organosolv eucalyptus lignin.[58,59] These results could indicate higher elimination of terminal hydroxymethyl groups or higher percentage of components such as stilbene or Hibbert's ketones in this fraction. The number and distribution of hydroxyl groups is important in the formation of intermolecular and intramolecular hydrogen bond interactions in lignin.[60] Aliphatic hydroxyl groups can form intermolecular hydrogen bonds and thus limit fusibility of lignin while phenolic hydroxyl groups give higher mobility to lignin. These intermolecular interactions are important for fiber formation during electrospinning and in the thermostabilizing step as they control rate of stabilization and crosslinking in the lignin.

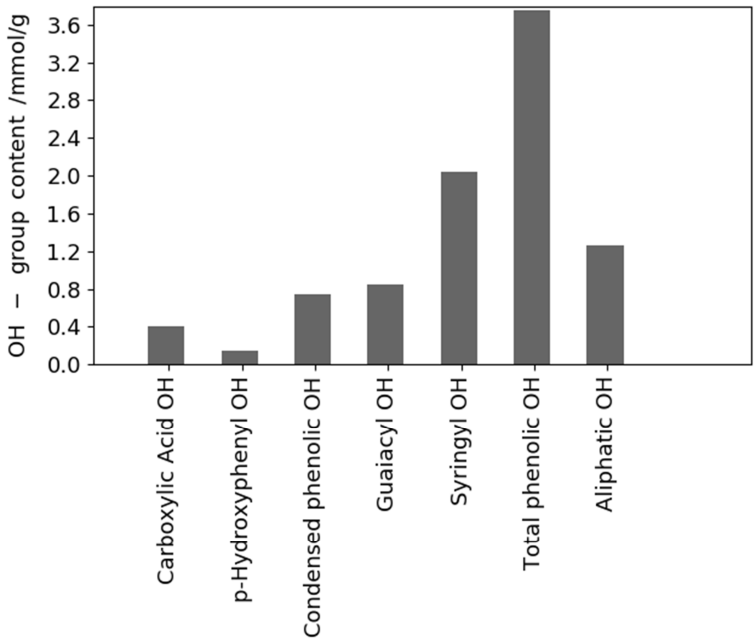

Figure 3 Distribution of phenolic moieties determined by ^{31}P NMR.

HSQC spectra and main correlation assignments of the lignin sample are shown in Figure 4. In the side chain region signals related to interunit linkages are predominant and signals related to carbohydrates are not discernible. This is consistent with compositional analysis which showed that the extracted lignin has a high purity. Main signals related to interunit linkages are β–O–4′ and resinol structures. Signals related to phenylcoumarans were not observed, while resinol shows strong signals. β–β linkages were also observed in the form of epiresinol as a result of base catalysed reactions.[61–63]

The phenylcoumarans are formed mainly from guaiacyl type units and on the other hand resinols are synthesized from syringyl units.[64] These observations could indicate a higher ratio of syringyl units in the fractionated lignin. In the aromatic region signals related to guaiacyl units, especially C_2–H_2 and C_6–H_6, are very weak which is an indication of condensation reactions in guaiacyl units or lower amount of guaiacyl units as it was observed in the side chain region.

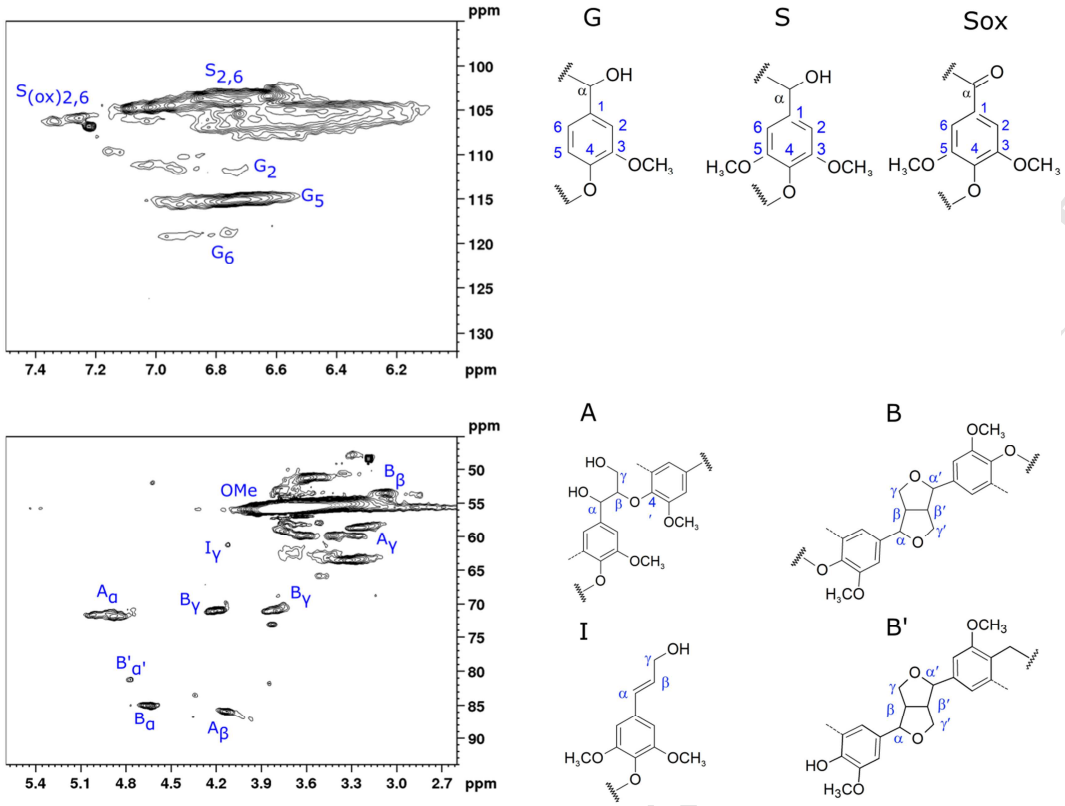

Figure 4 Aromatic (top) and side-chain (bottom) regions of the $^{13}C–^{1}H$ (HSQC) spectra of the eucalyptus Kraft lignin precursor: (G) guaiacyl (e.g. G2 signal from C on position 2); (S) syringyl; (S_{ox}) α-oxidized syringyl. (A) β–O–4′ aryl ether linkages (e.g. A_{α} signal from α-carbon); (B) resinol; (B') epiresinol; (I) cinnamyl alcohol end-groups; (OMe) methoxyl groups

3.2. Characterization of lignin fiber and carbon fiber mats

After preparation and characterization of the lignin precursor, fiber mats were produced by electrospinning the extracted eucalyptus Kraft lignin. The as-spun lignin fiber mats were then stabilized in air and carbonized in N_2. Additionally, some fiber mats were CO_2 activated. Due to the extraction, it was possible to electrospin fibers based on pure lignin without any additional synthetic high molecular weight polymer (e.g. PEO, PVA). Despite the low molecular weight of the lignin precursor (M_w = 1900 g/mol), compared with other polymer fibers, fiber formation during electrospinning was achieved as shown in the SEM micrographs in Figure 5.[65] The here

observed fiber formation is attributed to strong intermolecular interaction via hydrogen bonding and π-π-interactions between the lignin macromolecules in solution. Hence, the molecular weight is increased at high concentrations in solution. The resulting fiber mats consist of randomly entangled fibers with cylindrical shape. The as-spun fibers have an average diameter of 769 nm (Table 2) which is quite big compared to other studies confirming that intermolecular interactions must take place.[32,66] Additionally, the high polymer concentration in the solution (50 wt%) and the lack of additives (salts or co-polymers), generally decreasing fiber diameters, gives rise to fibers with big diameters.[66,67] After stabilization at 250 °C in air the overall fiber morphology does not change (no fusing of fibers).

Carbonization of the fibers at 900 °C leads to a decrease of approx. 100 nm to 567 nm. The additional activation step does not lead to a further decrease in fiber diameter.

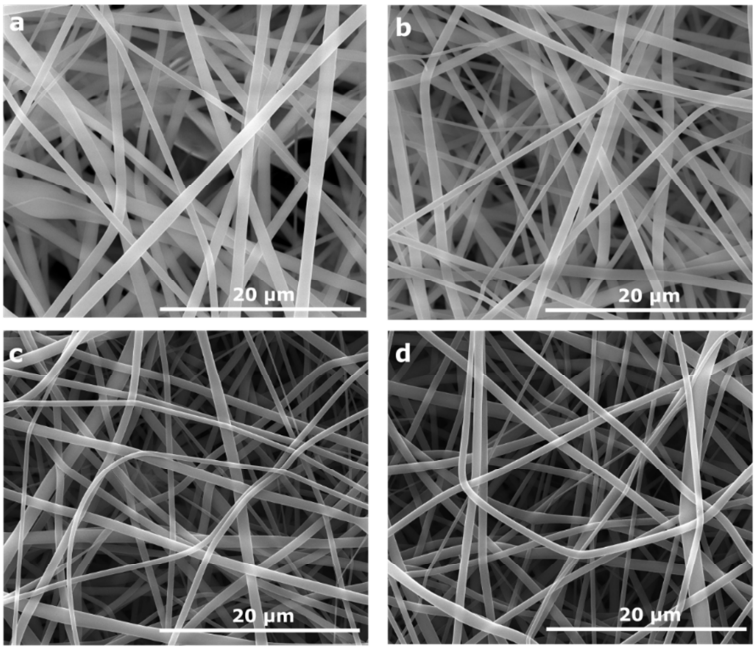

Figure 5 (a) as-spun fiber mat produced from a pure Kraft-lignin electrospinning solution, **(b)** stabilized fiber mat, **(c)** carbonized fiber mats (non-activated), and **(d)** activated for 60 min in CO_2.

Instead, the porosity increases dramatically which is discernible in the single fiber morphology analyzed by TEM (Figure 6).

Table 2 Average diameters of fibers and yields at all stages of the process chain.

Fiber	Average fiber diameter /nm	Standard deviation /nm	Yield /%
as-spun	769	258	-
stabilized	656	152	79
carbonized	567	132	42 (overall: 33.1)
CO_2-activated	566	177	75 (overall: 28.0)

The non-activated fiber (Figure 6a) is dense, whereas the CO_2-activated one contains additional porosity and hence appears less dense (6b).

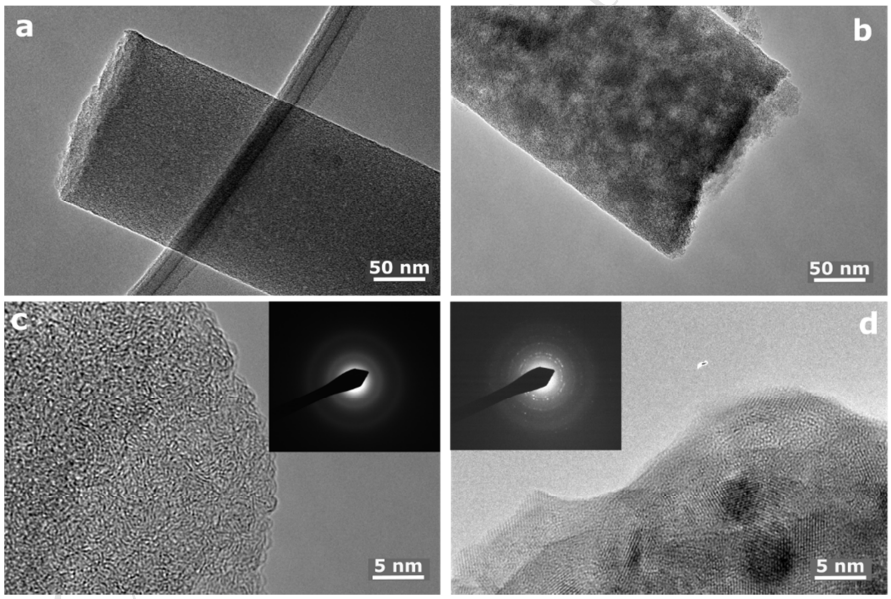

Figure 6 TEM image of **(a)** non-activated fiber, **(b)** CO_2-activated carbon fiber; electron diffraction of selected area on **(c)** non-activated, **(d)** CO_2-activated fiber.

Additionally, selected area electron diffraction (SAED) was carried out. Considering the short (30 min) carbonization time, low carbonization temperature (900 °C) and the disordered structure of the lignin precursor a low degree of graphitization is expected. This is confirmed by SAED

shown in Figure 6c. The rings in the diffraction pattern, however, indicate the presence of disordered graphene sheets. This is explained by the high degree of aromaticity in lignin determined by 2D NMR before. The additional one-hour treatment at 800 °C in CO_2 leads to partially graphitized domains in the carbon structure (Figure 6d). In addition to the diffraction rings there are diffraction spots superimposed indicative for polycrystalline graphite in the fiber. This might also be assigned to a leaching effect through CO_2 activation which exposes ordered domains which might be hidden in the dense matrix of the non-activated fibers.

The Raman spectra (Figure S6) of the non-activated and CO_2-activated samples show both D- and G- bands, indicating disordered carbon structures which was also concluded from the TEM micrographs. More details on the Raman analysis are given in the supplementary information (SI).

The results of the CO_2 and N_2 gas sorption experiments are shown in Figure 7a and b. The results clearly indicate that the CO_2 activation yields increasing porosity as the amount of adsorbed CO_2 and N_2 rises dramatically upon CO_2 activation.

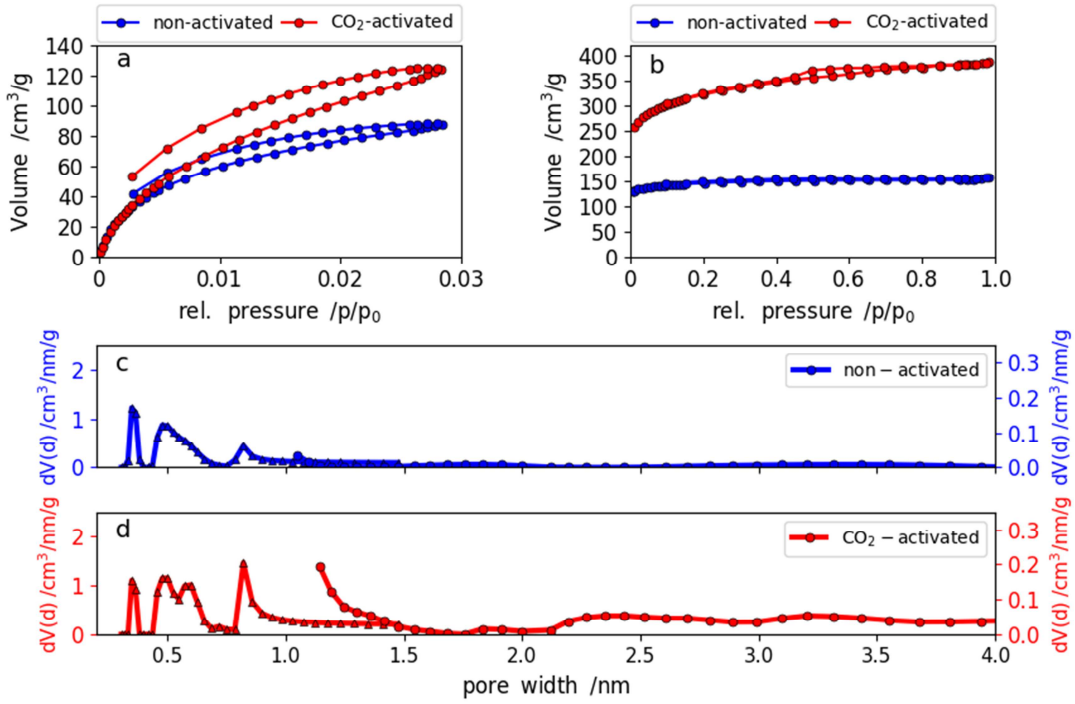

Figure 7 (a) CO_2 ad-/desorption isotherms of the non-activated (blue) and CO_2-activated (red) fiber mats **(b)** N_2 ad-/desorption isotherms of the non-activated (blue) and CO_2-activated (red) fiber mats. Pore size distributions calculated by DFT based on the adsorption isotherms for: **(c)** non-activated and **(d)** CO_2-activated fiber mats.

From both N_2 and CO_2 sorption measurements pore size distributions were generated by DFT models (NLDFT for CO_2 sorption and QSDFT for N_2 sorption).[68]

The resulting pore size distributions (PSDs) calculated by DFT based on the adsorption isotherms indicate that the non-activated sample contains a considerable amount of (ultra-)micropores (<1 nm) (Figure 7c). This was anticipated as the lignin precursor contains approximately 30 wt% of oxygen (Table 1) and high degree of disorder, hence a low packing density. The additional CO_2 activation effectively creates both meso (2 - 50 nm)- and micropores (<2 nm) (Figure 7d). This might take place by widening of the pre-existing (ultra-)micropores and additional creation of new (ultra-)micropores. This explanation is supported by the fact that the CO_2-activation did not decrease the overall fiber diameter (Table 2). Hence, the CO_2 oxidation might take place in

existing micropore space rather than uniformly on the external fiber surface. The increased porosity is also manifested in the values of specific surface area shown together with adsorbed gas volumes in Table S4.

The oxygen content on the fiber surface was determined by TPD and XPS. The results of the latter are given in the SI (Figure S7). The TPD spectra are shown in Figure 8. In general, the non-activated and CO_2-activated sample have very similar desorption rates of CO and CO_2. Overall, both samples desorb more CO (2562 and 2635 µmol/g) than CO_2 (860 and 896 µmol/g) (Table S5). From this, the total oxygen content was determined to be 6.9 wt% for the non-activated and 7.1 wt% for the CO_2-activated fibers.

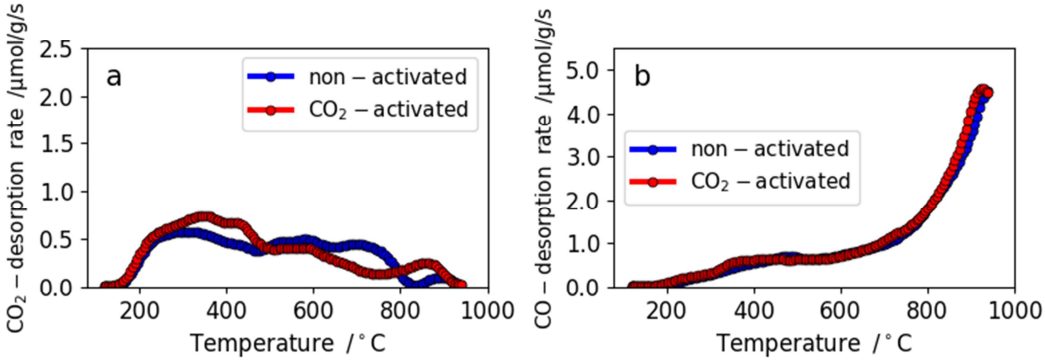

Figure 8 TPD spectra **(a)** CO_2 desorption rate and **(b)** CO desorption rate of non-activated (blue) and CO_2-activated sample (red) from TPD.

The evolution of CO_2 arises from carboxylic groups and their derivatives, such as lactones and anhydrides, whereas CO is associated with the decomposition of carbonyl groups, ethers and hydroxyl groups (e.g. phenols) groups.[14,69,70] It was shown that the CO-type oxygen groups have a positive effect on the capacitance in electric double layer capacitors (EDLCs) in basic electrolytes, whereas the CO_2-type oxygen groups are less stable and hence detrimental.[71] From ^{31}P NMR (Figure 3) and $^{13}C–^{1}H$ (HSQC) (Figure 4) spectra it is clear that the extracted

eucalyptus Kraft lignin precursor is rich of phenolic (especially: syringyl, aliphatic, guaiacyl and condensed groups) and ether bonds (especially: β-O-4' bonds). As determined by TPD, these oxygen functional groups are preserved in a reduced quantity (6.9/7.2 wt% to 30 wt%) upon thermal treatment which makes lignin a promising precursor for aqueous (especially basic) supercapacitors in terms of surface chemistry.

3.3. Testing the carbon fiber mats in supercapacitor

As shown in the model workflow in Figure 2, the last step is to test the lignin derived carbon fiber mats as free-standing electrodes in a symmetric supercapacitor (SC). Cyclic voltammetry at different scan rates was carried out on the non-activated and CO_2-activated carbon fiber mats in 6 M KOH (Figure 9). All voltammograms show the rectangular shape typical of electric double layer charge storage.[26,72] The CO_2 activated sample shows a slight curvature indicating pseudocapacitive contribution of the oxygen functional groups.[73] The absence of the contribution in the non-activated sample is assigned to the non-accessibility due to lacking porosity as the oxygen content only marginally changed upon CO_2 treatment. The voltammograms reveal that the increased porosity in the CO_2-activated mat translates into elevated capacitances. At low rates (5 and 50 mV/s) the difference between non-activated and CO_2-activated fiber mats is less pronounced. However, at 500 mV/s and 1 V/s, the non-activated sample shows a deformed rectangular shape indicating limited pore accessibility. This is well-explained by the gas sorption experiments which revealed that the short pyrolysis at 900 °C for 30 min effectively creates (ultra-)micropores, but hardly any meso- (2-50 nm) or bigger micropores (1-2 nm) as shown in Figure 7c.

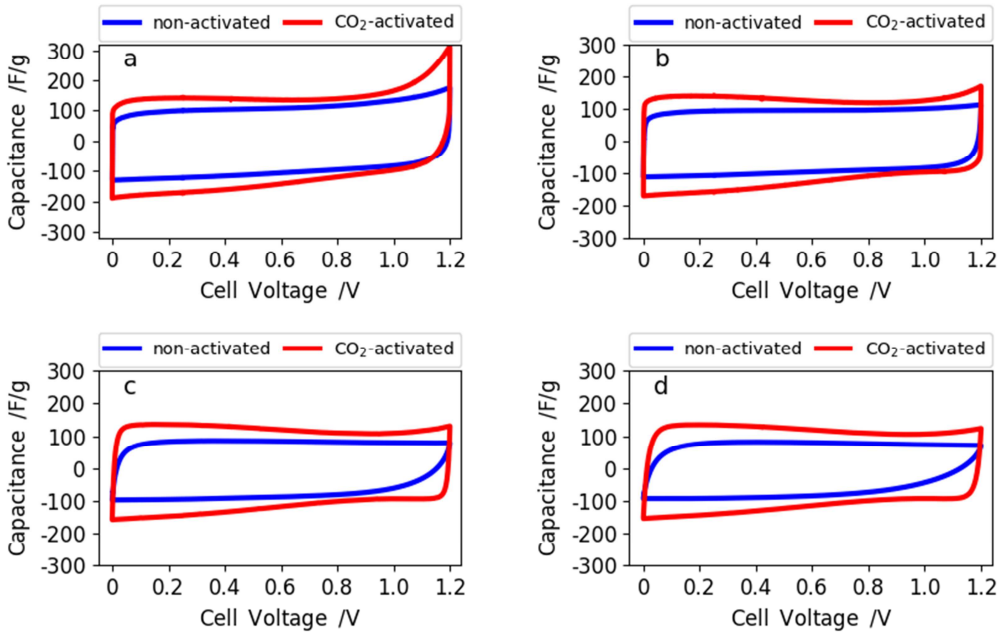

Figure 9 Cyclic voltammograms at scan rates of **(a)** 5, **(b)** 50, **(c)** 500 and **(d)** 1000 mV/s for the non-activated (blue) and CO_2-activated (red) carbon fiber electrodes.

The galvanostatic charge-discharge (GCD) curves at 0.25 A/g shown in Figure 10a exhibit the symmetric triangular shapes typical of EDLCs. As for the voltammograms, the GCD curves of the CO_2-activated sample shows a slight curvature indicating contribution from oxygen functional groups. The dependence of the specific gravimetric capacitances on current density was determined from the GCD curves at various current densities to investigate the rate capabilities (Figure 10b). Clearly, the CO_2-activation increases both the specific gravimetric capacitance which is 155 F/g at 0.1 A/g and the overall rate capabilities (113 F/g at 250 A/g) which can be assigned to the increased micro- and mesoporosity (Figure 7). The capacitance values attained are in line with other recent reports on lignin derived composite CFs (64 F/g, 83.3 F/g).[31,74] The leap in performance upon CO_2-activation is also shown in the corresponding Ragone plot in Figure 10c. Both energy and power density of the CO_2-activated

sample are considerably higher than of the non-activated sample. The difference between the samples is especially pronounced at high power density. The non-activated sample retains only 1.2 Wh/kg at 41 kW/kg, whereas the CO_2-activated sample achieves 4 Wh/kg at 52 kW/kg. This can be assigned to the presence of mesoporosity and accessibility of the stable basic oxygen functional groups in the CO_2-activated sample. The imaginary capacitance (C'') plotted as a function of frequency derived from impedance spectroscopy confirms this observation (Figure S8c). The maximum imaginary capacitance is located at the relaxation frequency, f_R, determining the characteristic time constant according to $\tau = (2\pi f R)^{-1}$. [75] In general the higher the time constant the lower the rate capability.[75] For the non-activated fiber mats, f_R= 0.68 Hz whereas for the CO_2-activated CFs, f_R= 14.5 Hz, hence the non-activated CFs exhibit a dramatically increased time constant of 0.23 s compared to the CO_2-activated sample (0.011 s). Further details on the impedance spectroscopy data may be found in the SI. Finally, the cyclability test at 5 A/g over 6000 cycles shows an interesting trend (Figure 10d). The CO_2-activated fiber mat exhibits a typical slight capacitance fade with increasing cycle number (94% after 6000 cycles). Contrarily, the non-activated fiber mat shows a slight increase in capacitance with cycle number. This is unusual and can be assigned to the low degree of pore accessibility and hence low pore penetration. However, with time (cycle number), a slight improvement of wettability by repetitive cycling is observed. The correlation between the mainly ultra-microporous PSD with low degree of accessibility and electrochemical performance is striking in this case.

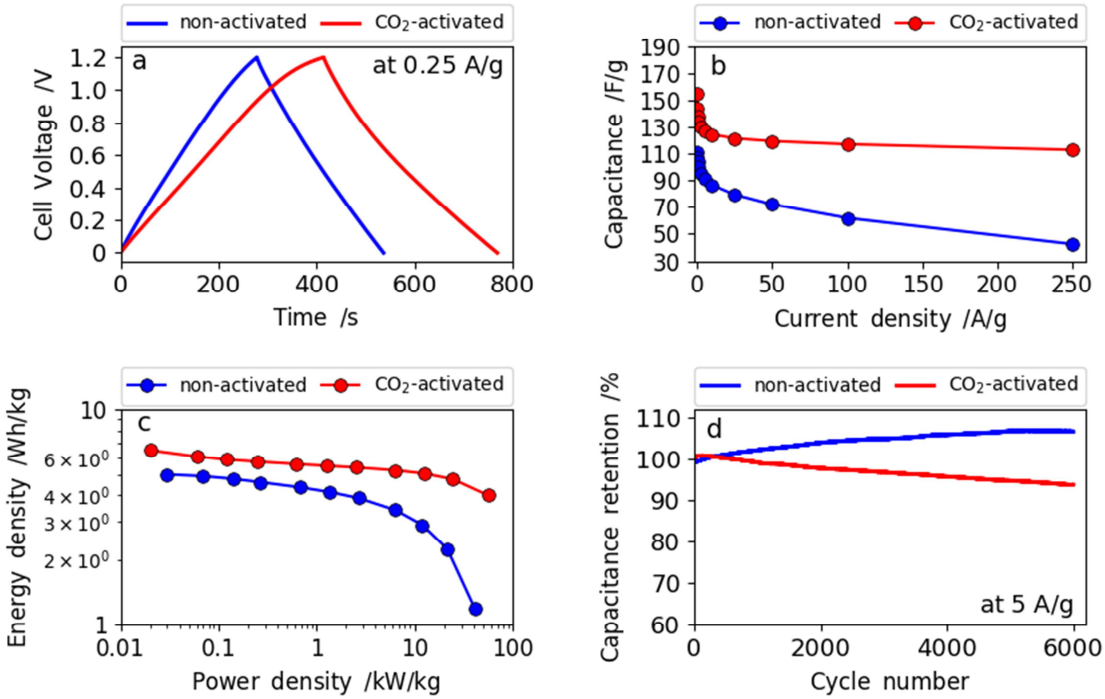

Figure 10 (a) Charge-discharge curves at 0.25 A/g, **(b)** dependence of specific gravimetric capacitance on current density, **(c)** Ragone plot and **(d)** capacitance retention for 6000 cycles at a current density of 5 A/g.

Due to the low density of activated carbon materials in general and especially of activated carbon fiber networks consideration of areal capacitance and volumetric energy/power density is of great importance (Figure 11). The differences in areal capacitance among the samples is similar to the specific gravimetric capacitance. However, the overall difference is less substantial.

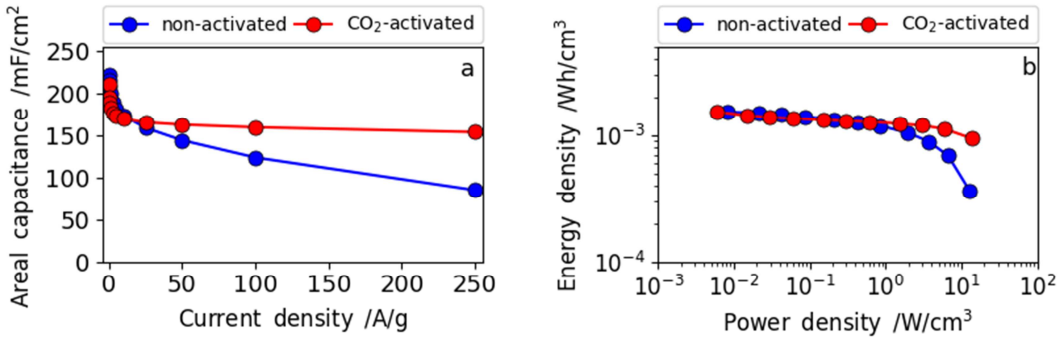

Figure 11 (a) Areal capacitance as a function of current density, **(b)** Ragone plot in volumetric measures.

This is also true for the Ragone plot in volumetric measures. This can be explained by the fact that the density of the CF networks is reduced by CO_2 activation which affects the volumetric measures negatively. Overall, the CO_2 activation is still beneficial in terms of rate capability as shown in Figure 11 a and b. This proves the importance of both gravimetric and volumetric measures for energy and power densities. Future works on carbon fiber networks for energy storage clearly need to focus on the densification in order to increase the volumetric energy and power densities. This work is currently in progress in our group.

Here, it was shown that it is possible to produce lignin-based carbon fiber mats from extracted eucalyptus Kraft lignin with high purity. The fiber formation from this low molecular weight polymer (1900 g/mol, PD = 1.5) in absence of any synthetic high molecular weight polymer is attributed to strong intermolecular interaction via H-bonding between ether bonds (esp. β-O-4) and hydroxyl groups (esp. aliphatic) and π-π interactions (various phenolic moieties) in the electrospinning solution at high lignin concentration. Through stabilization in air, carbonization in N_2 and activation in CO_2 it is possible to produce high performance free-standing carbon fiber mats from Kraft lignin without any additive. As shown the combination of high oxygen and carbon content and the high degree of aromaticity of the lignin precursor translate into (ultra-

)microporous oxygen functionalized carbon fibers with good yield. The mainly hydroxyl and ether groups of the initial precursor are preserved in a reduced quantity as beneficial basic oxygen groups in the final CFs. As a result, the lignin-based CF mats exhibit excellent performance in 6 M KOH. In order to improve volumetric energy/power densities the densification of these mats has to be achieved.

4. Conclusion

Here, the entire process from the precursor (Kraft lignin) to the application (supercapacitor) is described. By applying the workflow for the use of lignin as a precursor introduced here, it is possible to manufacture pure Kraft lignin derived carbon fibers without any additive (e.g. high molecular weight synthetic polymer). The fiber mats produced in this work were tested as free-standing electrodes in symmetric supercapacitors. The CO_2-activated fiber mats showed a high specific gravimetric capacitance of 155 F/g at 0.1 A/g, excellent rate capability with 113 F/g at 250 A/g when tested in 6 M KOH electrolyte and good capacitance retention of 94% after 6000 cycles. Thus, lignin is a promising precursor for the production of microporous, oxygen functionalized carbon fibers serving as free-standing electrodes in aqueous supercapacitors. In the future, these carbon fiber mats have to be densified in order to improve their volumetric energy/power density.

Acknowledgement

We thank Rise AB (RISE AB/Innventia AB) for providing the lignin precursor with characterization and for funding Philipp Schlee's PhD position. We would like to thank EPSRC (EP/R021554/1, EP/N509899/1, EP/P031323/1) for the financial support.

References

[1] J. Ralph, K. Lundquist, G. Brunow, F. Lu, H. Kim, P.F. Schatz, J.M. Marita, R.D. Hatfield, S.A. Ralph, J.H. Christensen, W. Boerjan, Lignins: Natural polymers from oxidative coupling of 4-hydroxyphenyl- propanoids, Phytochem. Rev. 3 (2004) 29–60. doi:10.1023/B:PHYT.0000047809.65444.a4.

[2] W. Boerjan, J. Ralph, M. Baucher, Lignin Biosynthesis, Annu. Rev. Plant Biol. 54 (2003) 519–546. doi:10.1146/annurev.arplant.54.031902.134938.

[3] K. Ruel, V. Chevalier-billosta, F. Guillemin, J. Berrio Sierra, J.-P. Joseleau, The wood cell wall at the ultrastructural scale - formation and topochemical organization, MADERAS Cienc. Y Tecnol. 8 (2006) 107–116. doi:10.4067/S0718-221X2006000200004.

[4] M.M. Campbell, R.R. Sederoff, Variation in Lignin Content and Composition, Plant Physiol. (1996) 3–13.

[5] R.L. Nicholson, Phenolic compounds and their role in disease resistance, Annu. Rev. Phytopathol. (1992) 369–389.

[6] P. Kenrick, P.R. Crane, The origin and early evolution of plants on land, Nature. 389 (1997) 33–39.

[7] C. Crestini, H. Lange, M. Sette, D.S. Argyropoulos, On the structure of softwood kraft lignin, Green Chem. 19 (2017) 4104–4121. doi:10.1039/C7GC01812F.

[8] S. Chatterjee, T. Saito, Lignin-Derived Advanced Carbon Materials, ChemSusChem. 8 (2015) 3941–3958. doi:10.1002/cssc.201500692.

[9] J. Zakzeski, P.C.A. Bruijnincx, A.L. Jongerius, B.M. Weckhuysen, The Catalytic Valorization of Lignin for the Production of Renewable Chemicals, (2010) 3552–3599.

[10] A. Van Heiningen, Converting a kraft pulp mill into an integrated forest biorefinery, Pulp Pap. Canada. 107 (2006) 38–43.

[11] A. Vishtal, A. Kraslawski, Challenges in industrial applications of technical lignins, BioResources. 6 (2011) 3547–3568. doi:10.15376/BIORES.6.3.3547-3568.

[12] M.M. Titirici, R.J. White, N. Brun, V.L. Budarin, D.S. Su, F. Del Monte, J.H. Clark, M.J. MacLachlan, Sustainable carbon materials, Chem. Soc. Rev. 44 (2015) 250–290. doi:10.1039/c4cs00232f.

[13] L. Jiang, L. Sheng, Z. Fan, Biomass-derived carbon materials with structural diversities and their applications in energy storage, Sci. China Mater. 61 (2018) 133–158. doi:10.1007/s40843-017-9169-4.

[14] S. Biniak, A. Świątkowski, M. Pakuła, Electrochemical Studies of Phenomena at Active Carbon- Electrolyte Solution Interfaces, in: L.R. RADOVIC (Ed.), Chem. Phys. Carbon, Pennsylvania, 2001: pp. 126–216.

[15] J.M. Tarascon, M. Armand, Issues and challenges facing rechargeable lithium batteries., Nature. 414 (2001) 359–367. doi:10.1038/35104644.

[16] B. Scrosati, J. Hassoun, Y.-K. Sun, Lithium-ion batteries. A look into the future, Energy Environ. Sci. 4 (2011) 3287. doi:10.1039/c1ee01388b.

[17] M.D. Slater, D. Kim, E. Lee, C.S. Johnson, Sodium-ion batteries, Adv. Funct. Mater. 23 (2013) 947–958. doi:10.1002/adfm.201200691.

[18] C. Tang, M.M. Titirici, Q. Zhang, A review of nanocarbons in energy electrocatalysis: Multifunctional substrates and highly active sites, J. Energy Chem. 26 (2017) 1077–1093. doi:10.1016/j.jechem.2017.08.008.

[19] Z. Chen, D. Higgins, A. Yu, L. Zhang, J. Zhang, A review on non-precious metal electrocatalysts for PEM fuel cells, Energy Environ. Sci. 4 (2011) 3167–3192. doi:10.1039/c0ee00558d.

[20] Y. Wang, K.S. Chen, J. Mishler, S.C. Cho, X.C. Adroher, A review of polymer electrolyte membrane fuel cells: Technology, applications, and needs on fundamental research, Appl. Energy. 88 (2011) 981–1007. doi:10.1016/j.apenergy.2010.09.030.

[21] J.S. Lee, S.T. Kim, R. Cao, N.S. Choi, M. Liu, K.T. Lee, J. Cho, Metal-air batteries with high energy density: Li-air versus Zn-air, Adv. Energy Mater. 1 (2011) 34–50. doi:10.1002/aenm.201000010.

[22] E. Frackowiak, Carbon materials for supercapacitor application, Phys. Chem. Chem. Phys. 9 (2007) 1774. doi:10.1039/b618139m.

[23] E. Frackowiak, F. Béguin, Carbon materials for the electrochemical storage of energy in capacitors, Carbon N. Y. 39 (2001) 937–950. doi:10.1016/S0008-6223(00)00183-4.

[24] J.R. Miller, A.F. Burke, J.R. Miller, A.F. Burke, A.F. Burke, Electrochemical capacitors: Challenges and opportunities for real-world applications, Electrochem. Soc. 17 (2008) 53–57. doi:10.1201/9781420069709.

[25] Z. Gao, Y. Zhang, N. Song, X. Li, Biomass-derived renewable carbon materials for electrochemical energy storage, Mater. Res. Lett. 5 (2017) 69–88. doi:10.1080/21663831.2016.1250834.

[26] T. Brousse, D. Bélanger, K. Chiba, M. Egashira, F. Favier, Materials for Electrochemical

Capacitors, in: C. Breitkopf, K. Swider-Lyons (Eds.), Handb. Electrochem. Energy, 2017: pp. 495–561.

[27] A. González, E. Goikolea, J.A. Barrena, R. Mysyk, Review on supercapacitors: Technologies and materials, Renew. Sustain. Energy Rev. 58 (2016) 1189–1206. doi:10.1016/j.rser.2015.12.249.

[28] Z. Wang, W. Zhang, X. Li, L. Gao, Recent progress in flexible energy storage materials for lithium-ion batteries and electrochemical capacitors: A review, J. Mater. Res. 31 (2016) 1648–1664. doi:10.1557/jmr.2016.195.

[29] S. Herou, P. Schlee, A. Belen Jorge, M. Titirici, Biomass-derived electrodes for flexible supercapacitors, Curr. Opin. Green Sustain. Chem. (2017) 2452–2236. doi:10.1016/.

[30] R. Berenguer, F.J. García-Mateos, R. Ruiz-Rosas, D. Cazorla-Amorós, E. Morallón, J. Rodríguez-Mirasol, T. Cordero, Biomass-derived binderless fibrous carbon electrodes for ultrafast energy storage, Green Chem. 18 (2016) 1506–1515. doi:10.1039/c5gc02409a.

[31] X. Ma, P. Kolla, Y. Zhao, A.L. Smirnova, H. Fong, Electrospun lignin-derived carbon nanofiber mats surface-decorated with MnO2 nanowhiskers as binder-free supercapacitor electrodes with high performance, J. Power Sources. 325 (2016) 541–548. doi:10.1016/j.jpowsour.2016.06.073.

[32] C. Ma, Z. Li, J. Li, Q. Fan, L. Wu, J. Shi, Y. Song, Lignin-based hierarchical porous carbon nanofiber films with superior performance in supercapacitors, Appl. Surf. Sci. 456 (2018) 568–576. doi:10.1016/j.apsusc.2018.06.189.

[33] F.J. García-Mateos, R. Berenguer, M.J. Valero-Romero, J. Rodríguez-Mirasol, T. Cordero, Phosphorus functionalization for the rapid preparation of highly nanoporous submicron-diameter carbon fibers by electrospinning of lignin solutions, J. Mater. Chem. A. 6 (2018)

1219–1233. doi:10.1039/c7ta08788h.

[34] D. Baker, O. Hosseinaei, High Glass Transition Lignins and Lignin Derivatives for the Manufacture of Carbon and Graphite Fibers, U.S. Patent 20140271443 A1, 2014.

[35] R. Mörck, H. Yoshida, K.P. Kringstad, Fractionation of Kraft Lignin by Successive Extraction with Organic Solvents. I. Functional Groups, 13C-NMR-Spectra and Molecular Weight Distributions, Holzforschung. 40 (1986) 51–60. doi:10.1515/hfsg.1988.42.2.111.

[36] TAPPI Standard T 211 om-12. Ash in wood, pulp, paper and paperboard: combustion at 525 °C, TAPPI Press, Atlanta, USA, 2012.

[37] TAPPI Standard T 222 om-11. Acid-insoluble lignin in wood and pulp, TAPPI Press, Atlanta, USA, 2011.

[38] TAPPI Useful Methods UM 250. Acid-soluble lignin in wood and pulp, TAPPI Press, Atlanta, USA, 2011.

[39] SCAN standard CM 71:09. Pulps – Carbohydrate content. Scandinavian Pulp, Paper and Board testing Committee, Stockholm, Sweden, 2009.

[40] R.K. Patterson, Automated Pregl-Dumas technique for determining total carbon, hydrogen, and nitrogen in atmospheric aerosols, Anal. Chem. 45 (1973) 605–609. doi:10.1021/ac60325a050.

[41] J. Rencoret, A. Gutiérrez, L. Nieto, J. Jiménez-Barbero, C.B. Faulds, H. Kim, J. Ralph, Á.T. Martínez, J.C. del Río, Lignin Composition and Structure in Young versus Adult Eucalyptus globulus Plants, Plant Physiol. 155 (2011) 667–682. doi:10.1104/pp.110.167254.

[42] D. Ibarra, M.I. Chávez, J. Rencoret, J.C. Del Río, A. Gutiérrez, J. Romero, S. Camarero, M.J. Martínez, J. Jiménez-Barbero, A.T. Martínez, Lignin Modification during Eucalyptus

globulus Kraft Pulping Followed by Totally Chlorine-Free Bleaching: A Two-Dimensional Nuclear Magnetic Resonance, Fourier Transform Infrared, and Pyrolysis−Gas Chromatography/Mass Spectrometry Study, J. Agric. Food Chem. 55 (2007) 3477–3490. doi:10.1021/jf063728t.

[43] S. Constant, H.L.J. Wienk, A.E. Frissen, P. de Peinder, R. Boelens, D.S. van Es, R.J.H. Grisel, B.M. Weckhuysen, W.J.J. Huijgen, R.J.A. Gosselink, P.C.A. Bruijnincx, New insights into the structure and composition of technical lignins: a comparative characterisation study, Green Chem. 18 (2016) 2651–2665. doi:10.1039/C5GC03043A.

[44] C.S. Lancefield, H.J. Wienk, R. Boelens, B.M. Weckhuysen, P.C.A. Bruijnincx, Identification of a diagnostic structural motif reveals a new reaction intermediate and condensation pathway in kraft lignin formation, Chem. Sci. 9 (2018) 6348–6360. doi:10.1039/c8sc02000k.

[45] A. Granata, D.S. Argyropoulos, 2-Chloro-4,4,5,5-tetramethyl-1,3,2-dioxaphospholane, a Reagent for the Accurate Determination of the Uncondensed and Condensed Phenolic Moieties in Lignins, J. Agric. Food Chem. 43 (1995) 1538–1544. doi:10.1021/jf00054a023.

[46] J. Rönnols, H. Schweinebarth, A. Jacobs, J. Stevanic Srndovic, A.-M. Olsson, A. Reimann, F. Aldaeus, Structural changes in softwood kraft lignin during nonoxidative thermal treatment, Nord. Pulp Pap. Res. J. 30 (2015) 550–561.

[47] O. Hosseinaei, D.P. Harper, J.J. Bozell, T.G. Rials, Role of Physicochemical Structure of Organosolv Hardwood and Herbaceous Lignins on Carbon Fiber Performance, ACS Sustain. Chem. Eng. 4 (2016) 5785–5798. doi:10.1021/acssuschemeng.6b01828.

[48] N.-E. El Mansouri, J. Salvadó, Structural characterization of technical lignins for the

production of adhesives: Application to lignosulfonate, kraft, soda-anthraquinone, organosolv and ethanol process lignins, Ind. Crops Prod. 24 (2006) 8–16. doi:http://dx.doi.org/10.1016/j.indcrop.2005.10.002.

[49] P. Mousavioun, W.O.S. Doherty, Chemical and thermal properties of fractionated bagasse soda lignin, Ind. Crops Prod. 31 (2010) 52–58. doi:https://doi.org/10.1016/j.indcrop.2009.09.001.

[50] Y. Tamai, H. Watanabe, A. Tomita, Catalytic gasification of carbon with steam, carbon dioxide and hydrogen, Carbon N. Y. 15 (1977) 103–106. doi:10.1016/0008-6223(77)90024-0.

[51] C.A. Mims, Catalytic Gasification of Carbon: Fundamentals and Mechanism, in: J. Lahaye, P. Ehrburger (Eds.), Fundam. Issues Control Carbon Gasif. React., Springer Netherlands, Dordrecht, 1991: pp. 383–407. doi:10.1007/978-94-011-3310-4_20.

[52] Y. Nordström, I. Norberg, E. Sjöholm, R. Drougge, A new softening agent for melt spinning of softwood kraft lignin, J. Appl. Polym. Sci. 129 (2013) 1274–1279. doi:10.1002/app.38795.

[53] T. V Lourençon, F.A. Hansel, T.A. da Silva, L.P. Ramos, G.I.B. de Muniz, W.L.E. Magalhães, Hardwood and softwood kraft lignins fractionation by simple sequential acid precipitation, Sep. Purif. Technol. 154 (2015) 82–88. doi:http://dx.doi.org/10.1016/j.seppur.2015.09.015.

[54] J.F. Kadla, S. Kubo, R.A. Venditti, R.D. Gilbert, A.L. Compere, W. Griffith, Lignin-based carbon fibers for composite fiber applications, Carbon N. Y. 40 (2002) 2913–2920. doi:10.1016/s0008-6223(02)00248-8.

[55] J.L. Braun, K.M. Holtman, J.F. Kadla, Lignin-based carbon fibers : Oxidative

thermostabilization of kraft lignin, Carbon N. Y. 43 (2005) 385–394. doi:10.1016/j.carbon.2004.09.027.

[56] H. Yoshida, R. Mörck, K.P. Kringstad, H. Hatakeyama, Fractionation of kraft lignin by successive extraction with organic solvents: II. Thermal properties of kraft lignin fractions, Holzforschung. 41 (1987) 171–176. doi:10.1515/hfsg.1987.41.3.171.

[57] O. Hosseinaei, D.P. Harper, J.J. Bozell, T.G. Rials, Improving processing and performance of pure lignin carbon fibers through hardwood and herbaceous lignin blends, Int. J. Mol. Sci. 18 (2017) 1410. doi:10.3390/ijms18071410.

[58] M. Balakshin, E. Capanema, On the Quantification of Lignin Hydroxyl Groups With 31P and 13C NMR Spectroscopy, J. Wood Chem. Technol. 35 (2015) 220–237. doi:10.1080/02773813.2014.928328.

[59] M. Yáñez-S, B. Matsuhiro, C. Nuñez, S. Pan, C.A. Hubbell, P. Sannigrahi, A.J. Ragauskas, Physicochemical characterization of ethanol organosolv lignin (EOL) from Eucalyptus globulus: Effect of extraction conditions on the molecular structure, Polym. Degrad. Stab. 110 (2014) 184–194. doi:https://doi.org/10.1016/j.polymdegradstab.2014.08.026.

[60] S. Kubo, J.F. Kadla, Hydrogen Bonding in Lignin: A Fourier Transform Infrared Model Compound Study, Biomacromolecules. 6 (2005) 2815–2821. doi:10.1021/bm050288q.

[61] J. Rönnols, A. Jacobs, F. Aldaeus, Consecutive determination of softwood kraft lignin structure and molar mass from NMR measurements, Holzforschung. 71 (2017) 563–570. doi:10.1515/hf-2016-0182.

[62] K. Lundquist, R. Stromberg, On the Occurrence of Structural Elements of the Lignan Type (β-β Structures) in Lignins The Crystal Structures of (+)-Pinoresinol and (±)-trans-3,4-

Divanillyltetrahydrofuran, Holzforschung. 42 (1988) 375–384. doi:10.1080/02773818708085260.

[63] C.S. Lancefield, G.M.M. Rashid, F. Bouxin, A. Wasak, W.C. Tu, J. Hallett, S. Zein, J. Rodríguez, S.D. Jackson, N.J. Westwood, T.D.H. Bugg, Investigation of the Chemocatalytic and Biocatalytic Valorization of a Range of Different Lignin Preparations: The Importance of β-O-4 Content, ACS Sustain. Chem. Eng. 4 (2016) 6921–6930. doi:10.1021/acssuschemeng.6b01855.

[64] H. Kim, J. Ralph, Solution-state 2D NMR of ball-milled plant cell wall gels in DMSO-d 6/pyridine-d5, Org. Biomol. Chem. 8 (2010) 576–591. doi:10.1039/b916070a.

[65] F.K. Ko, Y. Wan, Fundamentals of polymers, in: Introd. to Nanofiber Mater., Cambridge University Press, 2014: pp. 13–43.

[66] X. Zong, K. Kim, D. Fang, S. Ran, B.S. Hsiao, B. Chu, Structure and process relationship of electrospun bioabsorbable nanofiber membranes, Polymer (Guildf). 43 (2002) 4403–4412. doi:10.1016/S0032-3861(02)00275-6.

[67] A. Haider, S. Haider, I.K. Kang, A comprehensive review summarizing the effect of electrospinning parameters and potential applications of nanofibers in biomedical and biotechnology, Arab. J. Chem. (2015). doi:10.1016/j.arabjc.2015.11.015.

[68] J. Jagiello, M. Thommes, Comparison of DFT characterization methods based on N2, Ar, CO2, and H2 adsorption applied to carbons with various pore size distributions, Carbon N. Y. 42 (2004) 1225–1229. doi:10.1016/j.carbon.2004.01.022.

[69] M.C. Román-Martínez, D. Cazorla-Amorós, A. Linares-Solano, C.S.M. de Lecea, TPD and TPR characterization of carbonaceous supports and Pt/C catalysts, Carbon N. Y. 31 (1993) 895–902. doi:10.1016/0008-6223(93)90190-L.

[70] J.L. Figueiredo, M.F.R. Pereira, M.M.A. Freitas, J.J.M. Órfão, Modification of the surface chemistry of activated carbons, Carbon N. Y. 37 (1999) 1379–1389. doi:10.1016/S0008-6223(98)00333-9.

[71] M.J. Bleda-Martínez, J.A. Maciá-Agulló, D. Lozano-Castelló, E. Morallón, D. Cazorla-Amorós, A. Linares-Solano, Role of surface chemistry on electric double layer capacitance of carbon materials, Carbon N. Y. 43 (2005) 2677–2684. doi:10.1016/j.carbon.2005.05.027.

[72] F.B. E. Frackowiak, Carbon Materials for the Electrochemical Storage of Energy in capacitors, J. Carbon. 39 (2001) 937–950.

[73] L. Guan, L. Yu, G.Z. Chen, Capacitive and non-capacitive faradaic charge storage, Electrochim. Acta. 206 (2016) 464–478. doi:10.1016/j.electacta.2016.01.213.

[74] C. Lai, Z. Zhou, L. Zhang, X. Wang, Q. Zhou, Y. Zhao, Y. Wang, X.F. Wu, Z. Zhu, H. Fong, Free-standing and mechanically flexible mats consisting of electrospun carbon nanofibers made from a natural product of alkali lignin as binder-free electrodes for high-performance supercapacitors, J. Power Sources. 247 (2014) 134–141. doi:10.1016/j.jpowsour.2013.08.082.

[75] P.L. Taberna, P. Simon, J.F. Fauvarque, Electrochemical Characteristics and Impedance Spectroscopy Studies of Carbon-Carbon Supercapacitors, J. Electrochem. Soc. 150 (2003) A292. doi:10.1149/1.1543948.